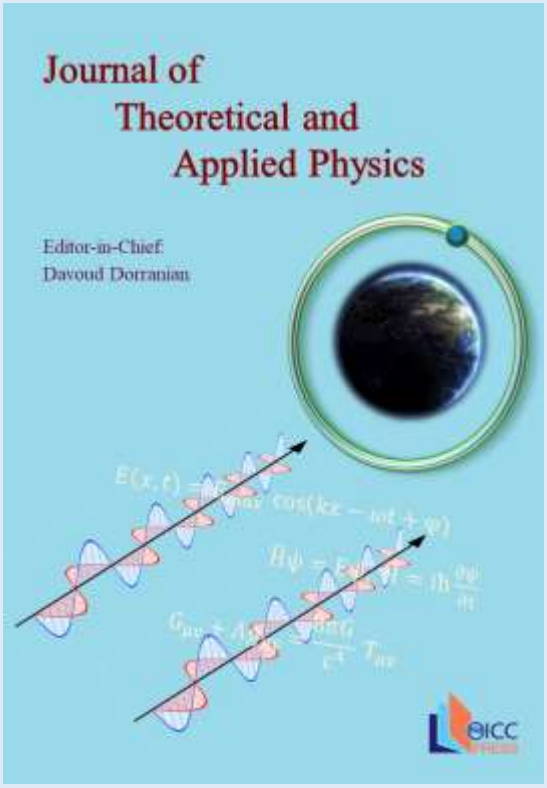

ACCEPTED PAPER

Particle acceleration by three-dimensional asymmetric current sheet

Zahra Akbari, Mahboub Hosseinpour *, Mohammad Ali Mohammadi

Faculty of Physics, University of Tabriz, Tabriz, Iran

hosseinpour@tabrizu.ac.ir

Received: 12 December 2022;

Accepted: 14 April 2023;

http://dx.doi.org/10.57647/J.JTAP.2023.1703.33

Particle acceleration by three-dimensional asymmetric current sheet

Zahra Akbari[1], Mahboub Hosseinpour[1,*], Mohammad Ali Mohammadi[1]

Faculty of Physics, University of Tabriz, Iran

Abstract

Magnetic reconnection is known as an essential process to convert stored energy of magnetic field into the kinetic, thermal energy of plasma and the acceleration of charged particles in astrophysical and space plasmas. In this paper, we investigate some features of test particle acceleration during spine reconnection with an asymmetric current sheet. To do so, we study first the acceleration features of a test-particle and then discuss acceleration of a randomly injected population of 10,000 protons in the vicinity of a null point with input parameters for the solar corona. It is shown that protons are accelerated up to tens of keV and even higher kinetic energies, either along the spine axis or on the fan surface along specified lines. Also, we discuss the variation of energy spectra for different strengths of the electric and magnetic field amplitudes.

Keywords

magnetic reconnection, asymmetric current sheet, particle acceleration.

[1] Faculty of Physics, University of Tabriz, Iran
***Corresponding author:** hosseinpour@tabrizu.ac.ir

1. Introduction

A ubiquitous and frequent dynamic process which occurs in an almost ideal plasma due to non-ideal magnetohydrodynamic (MHD) effects such as the plasma resistivity is magnetic reconnection. This phenomenon is responsible for a broad range of dynamic events such as conversion of magnetic energy to the plasma kinetic, thermal and non-thermal energies by the change of magnetic field topology in astrophysical and space plasmas such as the solar corona [1-4]. Also, it is considered to be an essential mechanism for particle acceleration, in particular, in solar flares [5-11]. The most important consequences of two-dimensional (2D) magnetic reconnection studies involve a magnetic null point named X-point, where the magnitude of magnetic field is supposed to be zero. However, the later studies revealed a complex picture of three-dimensional (3D) solar magnetic fields and the occurrence of magnetic reconnection in a magnetic topology with and without null points [12-15]. A null point reconnection with its various models (torsional spine and torsional fan reconnections); non-null point reconnection and separator reconnection are the most important regimes of 3D magnetic reconnection [14-22]. Torsional spine (fan) reconnection occurs due to a rotational disturbance around the fan plane (spine) forming a strong current aligned to the spine axis (fan plane). Non-null point reconnection takes place in the absence of a null point and requires a localized non-ideal region together with a non-zero electric field component parallel to the magnetic field. Separator reconnection occurs in current layers around separators [17,23,24].

It is worth to note that the most of magnetic reconnection studies of both two and three dimensions focus on symmetric configurations. Asymmetric reconnections, however, are likely to be more real and natural. Frequently, spatially asymmetric magnetic fields around reconnection sites in the atmosphere of the Sun have been observed [25-28]. Recently, asymmetric magnetic reconnection is considered in some literatures. In 2D configurations, the asymmetric upstream/downstream densities, magnetic field strengths, the exhaust velocities, the thickness of current sheet and the effects of asymmetry on the rate of reconnection have been considered. Due to the variations of magnetic field geometry, the null point reconnection in 3D can become asymmetric either in the fields around a null point or in the corresponding electric currents. Also, such an asymmetric current sheet can be formed even with an initially symmetric null and a homogeneous plasma [29,30]. It is

shown that the current sheet near the null point must be asymmetric to accommodate the observed asymmetric flows in the vicinity of the null point [29]. The symmetry and asymmetry of the magnetic field in the vicinity of a magnetic null point have been investigated and their profound effect on the geometry and the rate of any associated reconnection region have been reported [31]. Already, Galsgaard and Pontin [32] have investigated the importance of magnetic field topology in determining the accumulation point of the electric current in a single 3D null point.

It is believed that magnetic reconnection can efficiently accelerate particles up to highly relativistic energies in astrophysical plasmas, in particular, in the solar corona environment. There are three important mechanisms for particle acceleration which categorized as the acceleration by shocks, stochastic acceleration by waves and by direct electric fields due to magnetic reconnection [33-35]. There is a wealthy supply of data from RHESSI observations on the particle acceleration events in the solar corona which show that a fraction of $10\% - 50\%$ of transferred energy has been detected in electrons of some flares with energies about $20 - 100\ keV$ [36]. Also, Lin et al. (2003) [37] has observed the accelerated electrons and protons up to energies of a few MeV and even higher during the impulsive phase of an intense solar flare.

Furthermore, asymmetric reconnection has been observationally reported in many contexts, for example, in situ measurements of magnetic reconnection in the Earth's magnetotail structure [38]. Also, magnetospheric multiscale observations of an electron-scale current sheet and the electron outflow jet for asymmetric reconnection at the subsolar magnetopause shows the jet is unstable to an electrostatic instability which generates intense waves with parallel electric field amplitudes reaching up to $300\ MV/m$ and electric potentials up to 20% of the electron thermal energy [39].

Recently, particle acceleration in the vicinity of a null point for spine and fan reconnection regimes were studied by Dalla and Browning (2005, 2006, 2008) [40-42]. They showed that the spine reconnection is more efficient than the fan reconnection in accelerating charged particles to kinetic energies of the order of MeV. Also, proton and electron acceleration investigations in a nonneutral reconnecting current sheet showed that electrons and protons were accelerated to the energies of $10 - 100\ keV$ and $100 - 400\ keV$, respectively [43,44]. Moreover, two important types of 3D symmetric null point

reconnection regimes named torsional spine and torsional fan reconnections by a test particle approach were investigated [45-47]. It has been shown that proton acceleration up to MeV and even higher kinetic energies for typical parameters of the solar corona takes place in less than a few milliseconds [45-47]. On the other hand, it has been shown that the trajectory of an accelerated proton either along the spine axis or on the fan plane significantly depends on its initial location. In fact, protons are accelerated along the magnetic field lines away from the non-null point only at azimuthal angles where the magnitude of the electric field is strongest, and therefore particles obtain kinetic energies of the order of thousands of MeV and even higher. However, comparison shows that a non-null magnetic reconnection is more efficient in accelerating protons to GeV energies than a null-point reconnection [48]. In our most recent study [49], the trajectory and energy distribution of accelerated protons were investigated in the presence of magnetic and electric fields of a particular 3D reconnection model, named flux tube disconnection with an O-type topology [21]. We concluded that the acceleration of an injected proton to highly relativistic kinetic energies can be observed close to the origin of the diffusion region and the particle's trajectory is along the magnetic field lines. Also, we showed that the electric drift velocity reaches its maximum magnitude at a particular radial point and the efficient acceleration is experienced at that point.

Since the naturally occurring magnetic reconnection is basically asymmetric, now it will be interesting to study the acceleration of particles in various regimes of reconnection with some asymmetries such as magnetic field asymmetry, current sheet asymmetry. Here, we are interested to investigate the particle acceleration scenario using the test-particle approach in an asymmetric current sheet around 3D null point. Thus, by considering a kinematic model of asymmetric spine reconnection given by Wyper and Jain (2013) [47], the trajectory and energy distribution are investigated first for a proton test-particle and then for a population of 10,000 protons which are randomly distributed within a cubic spatial space around the null point with typical parameters for the solar corona. In the following sections, we consider the configuration and properties of an asymmetric reconnection model and give a description of the trajectory code in sec. 2, while we discuss the results in sec. 3. A brief conclusion is presented in Sec. 4.

2. The model of spine reconnection with asymmetric current sheet and the "trajectory code"

The aim of this study is to investigate particle acceleration in a particular model of asymmetric magnetic reconnection based on the analytical solution of Wyper and Jain (2013) [29] which is a linear potential with radially symmetric magnetic null field as the background field and with a localized perturbation field. Here the symmetric magnetic field solution of the following steady-state resistive MHD equations

$$\mathbf{E} + \mathbf{V} \times \mathbf{B} = \eta \mathbf{J}, \qquad (1)$$

$$\nabla \times \mathbf{E} = 0, \qquad (2)$$

$$\nabla \times \mathbf{B} = \mu_0 \mathbf{J}, \qquad (3)$$

$$\nabla . \mathbf{B} = 0, \qquad (4)$$

in the cylindrical coordinates is in the form of

$$\mathbf{B_0} = \frac{b_0}{L_0}(r, 0, -2z),$$

with B_1 added as a perturbed field localized in r and is of the form

$$\mathbf{B_1} = F(r, \varphi)\hat{\mathbf{z}} = \frac{jb_0}{L_0} f(\varphi) r \exp(-\frac{r^2}{h(\varphi)^2})\hat{\mathbf{z}},$$

so that the total magnetic field is given by

$$\mathbf{B} = \mathbf{B_0} + \mathbf{B_1}. \qquad (5)$$

Here j is a dimensionless constant to control the magnitude of $\mathbf{B_1}$ and b_0 and L_0 are the field strength on the boundary and the length scale, respectively. Moreover, f, and h functions dependent only on φ (azimuthal angle) which are given below. With the choice of localized non-uniform resistivity of the form

$$\eta = \eta_0 \ exp(-\frac{(Zr^2)^2}{k^6}),$$

in which k determines the level of localization. We obtain the electric potential of the form

$$\Phi = -\frac{j\eta b_0}{\mu_0 L_0}[\frac{\sqrt{\pi}h(\varphi)}{2} f'(\varphi)(r)], \qquad (6)$$

We assume

$$f(\varphi) = \sin(\varphi) \ ,$$

$$h(\varphi) = L(1 + m \ sin(\varphi)), \qquad (7)$$

where m is the parameter which determines various degrees of asymmetry to the magnetic field and is limited to $0 < m < 1$. In Figure 1, we illustrate some magnetic field lines in three dimensions with $b_0 = L_0 = j = 1$ and $m = 0.5$. Also, the asymmetric degree of current sheet and the electric field is determined by m. So, the symmetric case is recovered by $m = 0$. The vector plot of the electric current density according to Eq. (3) is shown in the $x - y$ plane (fan plane) in Figure 2 (with $m = 0$ (a) and $m = 0.5$ (b)). It is seen from Figure 2 (a) that the current rings in both sides of $y = 0$ axis on the fan plane are symmetric while asymmetric current rings can be seen in Figure 2 (b) where $m = 0.5$. Using Eqs. (6), (7) and the expression $\mathbf{E} = -\nabla\Phi$, the electric field components can be obtained as

$$E_r = e_0[\cos(\varphi) + 2m\cos(\varphi)\sin(\varphi)L^2(1 + m\sin(\varphi))^3 \ r^2]$$

$$\times \exp(-\frac{r^2}{L^2(1 + m\sin(\varphi))^2}),$$

$$E_\varphi = +\frac{e_0}{r}\{(\frac{\sqrt{\pi}L}{2}(\frac{r}{L(1+m\sin(\varphi))})$$

$$\times (m\cos^2(\varphi) - (1 + m\sin(\varphi))\sin(\varphi)))$$

$$+(-\frac{mr\cos^2(\varphi)}{1+m\sin(\varphi)} + \frac{mr(\sin^2(\varphi)-cos^2(\varphi))}{L(1+m\sin(\varphi))}$$

$$+\frac{m^2 r\cos^2(\varphi)\sin(\varphi)}{L(1+m\sin(\varphi))^2}\left(1-\frac{2r^2}{L^2(1+m\sin(\varphi))^2}\right)$$

$$+\frac{mr\cos(\varphi)}{1+m\sin(\varphi)}\exp\left(-\frac{r^2}{L^2(1+m\sin(\varphi))^2}\right)$$

$$-\frac{\sqrt{\pi}Lm\cos(\varphi)}{2}\left(\frac{r}{L(1+m\sin(\varphi))}\right)\}$$

$$E_z = 0, \qquad (8)$$

with $e_0 = j\eta b_0/\mu_0 L_0$. Throughout the paper, we put $L_0 = 1, \mu_0 = 4\pi \times 10^{-7}\ H/m$, $\eta = 1,\ j = 1,\ L = 1,\ B_0' = 0.01\ T,\ E_0 = 1\ kV/m$ and $L' = 10\ km$ (B_0', E_0 and L' are typical magnetic and electric field strengths, and the length scale in the solar corona, respectively).

Now, having the electric and magnetic fields **E** and **B** given by Eqs. (8) and (5), the particle's trajectory can be obtained by solving the following equations of motion

$$\frac{d\mathbf{x}}{dt} = \frac{\mathbf{p}}{m_0\gamma}, \qquad (9)$$

$$\frac{d\mathbf{p}}{dt} = q\left(\mathbf{E} + \frac{\mathbf{p}}{m_0\gamma} \times \mathbf{B}\right). \qquad (10)$$

Here x and p are the particle's position and momentum vectors, q and m_0 are its charge and rest mass, $\gamma = 1/\sqrt{1 - v^2/c^2}$ is the Lorentz factor, and c is the speed of light. Eqs. (9) and (10) are numerically solved by the trajectory code with length scales, the magnetic field and time normalized to the characteristic length $L' = 10\ km$ corresponding to a typical scale in the solar corona, a typical magnetic field of an active region, $B_0 = 0.01\ T$, and the non-relativistic gyroperiod of a proton, namely, $T = 2\pi m_0/(qB_0)$ i.e., $T \approx 6.5\ \mu s$, respectively.

3. Results and discussion

To investigate the features of particle acceleration in asymmetric spine reconnection, we study the trajectory of a test particle injected initially in some different positions. Numerical

solution of Eqs. (9) and (10) give the position and momentum (velocity) of the particle at any running time. In Figure 3, trajectories of a proton with seven different injection positions from the second and forth quadrants listed in table 1 are shown in the $x - z$ plane. Also, the pitch angle and azimuthal angle of the injected particle for all cases are 90° and 45°, respectively. Note that the initial kinetic energy of the injected particle for all cases is 100 eV and the total running time of the code is set to be $T_{fin} = 2000$, corresponding to $\sim 13ms$. Trajectories of a proton for other seven injection positions from the first and third quadrants listed in table 2 are plotted in the $x - y$ plane in Figure 4. The background pale lines indicate projections of magnetic field lines in both figures. It is seen that the trajectory of a proton strongly depends to its initial position. A proton with an initial position from the second and forth quadrants of top and below of $z = 0$ (fan plane) moves along the spine receding from the null or close to the first and third bisectors. However, a proton with an initial position from the first and third quadrants moves along the first and third bisectors. In fact, the trajectory of particles is mainly determined by the electric field pattern. Figure 5 (a) shows the electric field on fan plane ($z = 0$) is directed out from the null and the spine and parallel to $z = 0$ axis. Also, it is symmetrically independent of height and decreases with increasing of distance from the null on the fan plane as well as on the other $z = constant$. with direction toward to the fan plane. While, Figure 5 (b) shows that the direction of the electric field remains outward of the spine and loses its direction toward the fan plane. It is now directed parallel to the fan plane in the first and third quadrants while it directs to the first and third bisectors in the second and forth quadrants. Besides, we see that the electric field decreases as the height increases.

Moreover, the final kinetic energy of an accelerated particle dependent to its initial position. The kinetic energy of the relativistic particle is calculated from the momentum through equation $E_k = \sqrt{c^2p^2 + m_0^2c^4} - m_0c^2$, which reduces to $E_k = 1/2\, m_0v^2$ in the nonrelativistic case. We see from Figure 6 that by increasing the injection radial distance from the null (or the spine axis) at a constant height, $z = 0.3$, the kinetic energy decreases. Here, initial pitch angle, azimuthal angle, initial energy and the total running time of the code are as the same as before. Time variation of kinetic energy of the particle for four different initial positions are listed in table 3.

Now, we randomly inject a population of 10,000 protons inside a cubic region of $1 < x < 1, 1 < y < 1, 1 < z < 1$ with dimensionless units around the null point at $t = 0$. The initial velocity of the injected particles is isotropically randomized according to a Maxwellian distribution with a mean temperature of $T = 86\ eV$ ($\sim 10^6\ K$) corresponding to the mean thermal speed of $v_{ave} \sim 1.3 \times 10^5\ m/s$. Keeping all other parameters, the same as before with $T_{fin} = 4000$ and $m = 0.5$, Figures 7 and 8 show the final position of the population of the particles in three and two dimensions, respectively. Figure 9 indicates that almost 70% of particles accelerated parallel to the magnetic field lines with pitch angle less than 6° and 23% are accelerated anti-parallel to the magnetic field lines with pitch angle more than 175°. Furthermore, our study on the effect of varying m as a parameter of asymmetry shows that with increasing m from 0 to 1, the percentage of particles tend to move anti-parallel to the magnetic field lines increases. As seen from Figure 10 (a), we see that more than ~ 99% of the particles are accelerated parallel to magnetic field lines when m = 0, Whilst, less than ~ 60% of the particles keep moving parallel to magnetic field lines when $m = 1$ (Figure 10 (b)).

The energy distribution of the accelerated particles (the number of particles in each energy range divided by the total number of particles, fn) is plotted in Figure 11 with three values of m. Figure 11 shows that with m = 0, there is only one peak, while, increasing the magnitude of m results in appearance of another peak in lower energies. Almost all of the particle population (~ 96%) gains kinetic energies between 10 keV and $1MeV$ with a peak about ~ 65 keV for $m = 0$.

For m = 1 the first peak occurs at ~ 40 eV and the second peak at ~ 250 keV. Additionally, it is seen that increasing the level of asymmetry shifts the position of the second peak towards much higher kinetic energies. Finally, we study the effect of the electric and magnetic field amplitudes, E_0 and B_0' on the variation of energy distribution. These variations are illustrated in Figures 12 and 13 for four different values of $E_0 = 0.1, 1, 10, 20\ kV/m$, with $B_0' = 0.01\ T$ and for three different values of $B_0' = 0.001, 0.01, 0.1T;\ T$ with $E_0 = 1\ kV/m$, respectively. The strength of the electric field magnitude has been measured for solar flares in many studies. For example, observation of an electric field as high as 17 kV/m in postflare coronal loops is reported by Foukal et al.

(1983) [50]. Even more intensive electric fields (up to $70\ kV/m$) has been measured by Davis (1977) [51]. Besides, the findings of Foukal et al. (1987) [52] from two eruptive events show an electric field less than $1\ kV/m$ in such structures and about $4\ kV/m$ in a postflare loop. Also, the intensity of flare electric field estimation by Pudovkin et al. (1998) [53] is approximately $0.1 - 0.3\ kV/m$. According to Figure 12, as E_0 increases about two orders of magnitude, the peak of energy distribution shifts about two orders of magnitude to higher energies from $\sim 160\ keV$ to $\sim 16\ MeV$. There is also a reduction in the fraction of the particle population with lower kinetic energies. Furthermore, Figure 13, shows that the increase of magnetic field magnitude has no significant influence on the energy distribution and its corresponding peak.

4. Conclusions

Accelerated charged particles are thought to be a significant signature of magnetic reconnection in the astrophysical and space plasmas, in particular, in solar flares. Therefore, magnetic reconnection is considered as an important mechanism of particle acceleration in solar fares. The aim of the current study was to show some acceleration features of a single charged particle (proton) and also a population of many test particles in the presence of static electric and magnetic fields associated with asymmetric spine reconnection, a more realistic regime of 3D magnetic reconnection at a null point. The initial velocities of particles were randomly distributed according to a Maxwellian distribution. Numerical solution of the equations of motion showed that almost all of the injected particles around the null point are accelerated along the magnetic field lines, either along the spine or close to the bisector lines of quadrants. The trajectory depends on the parameter *m* which applies a certain amount of perturbation to the magnetic field and in the generated current sheet. According to our study, for $m = 0$, almost ~ 99% of the particles are accelerated parallel to magnetic field lines and for $m = 1$, about ~ 24% of the particles move anti-parallel to magnetic field lines. Note that our study considers three values of *m* but, the results are reported only for $m = 0.5$. According to the final position distribution especially in two dimensions (Figure 8), it is seen that most of particles accelerated along the fan plane and gain higher energies than particles which are accelerated along the spine. Unlike the results of our previous work on particle acceleration in torsional spine reconnection where jets of

accelerated particles were found [54], the final distribution in asymmetric spine reconnection does not show such jets of particles. Investigation about the final kinetic energy of a single particle with various injection positions for proton indicates that the final energy decreases with increasing injection radial distance from the null and spine axis for a constant height, z, as expected from the variation of the strength of the electric field. However, almost all of the particles ($\sim 96\%$) with $E_0 = 1\, kV/m$ and $B_0' = 0.01\, T$, obtain high energies, $10\, keV - 400\, keV$. We concluded that increasing the amplitude of electric field by two orders of magnitude results in the shift of energy peak location by two orders. However, there is no considerable variation for energy distribution by variation of the magnetic field magnitude. Here we investigated 3D null point magnetic reconnection called spine reconnection with an asymmetric current sheet, where the electric and magnetic fields were considered to be static. More realistic models need to take into account the transient time-dependent fields.

References

[1] J. Birn and E. R. Priest. *Cambridge University Press, Cambridge* (2007).

[2] E. R. Priest and T. G. Forbes. *Cambridge University Press, Cambridge* (2000).

[3] M. Yamada, R. Kulsrud and H. Ji. *Reviews of Modern Physics* **82** (2010) 603.

[4] E.G. Zweibel and M. Yamada. *Annual Review of Astronomy and Astrophysics* **47** (2009) 291.

[5] A. O. Benz, P. C. Grigis and M. Battaglia. *Plasma Physics and Controlled Fusion* **48** (2006) B115.

[6] R. G. Giovanelli. *Nature* **158** (1946) 81.

[7] M. L. Goldstein, W. H. Matthaeus and J. J. Ambrosiano. *Geophysical Research Letters* **13** (1986) 205.

[8] P. Helander, L.-G. Eriksson, R. J. Akers, C. Byrom, C. G. Gimblett and M. R. Tournianski. *Physical Review Letters* **89** (2002) 235002.

[9] K. Knizhnik, M. Swisdak and J. F. Drake. *The Astrophysical Journal Letters* **743** (2011) L35.

[10] R. P. Lin. *Space Science Reviews* **159** (2011) 421.

[11] V. V. Zharkova, K. Arzner, A. O. Benz, P. Browning, C. Dauphin, A. G. Emslie, L. Fletcher, E. P. Kontar, G. Mann, M. Onofri, V. Petrosian, R. Turkmani, N. Vilmer and L. Vlahos. *Space Science Reviews* **159** (2011) 357.

[12] D.I. Pontin. *Advances in Space Research* **47** (2011) 1508.

[13] D. I. Pontin, A. K. Al-Hachami and K. Galsgaard. *Astronomy and Astrophysics* **533** (2011) A78.

[14] E. R. Priest and D. I. Pontin. *Physics of Plasmas* **16** (2009) 122101.

[15] E. R. Priest and V.S. Titov. *Philosophical Transactions of the Royal Society A* **354** (1996) 2951.

[16] K. Galsgaard, E. R. Priest and V. S. Titov. *Journal of Geophysical Research: Space Physics* **108** (2003) 1042.

[17] Y.-T. Lau and J. M. Finn. *Astrophysical Journal* **350** (1990) 672.

[18] D. W. Longcope and S. C. Cowley. *Physics of Plasmas* **3** (1996) 2885.

[19] D. I. Pontin and K. Galsgaard. *Journal of Geophysical Research: Space Physics* **112** (2007) A03103.

[20] E.R. Priest and T.G. Forbes. *Journal of Geophysical Research: Space Physics* **97** (1992) 1521.

[21] A. L. Wilmot-Smith and E. R. Priest. *Physics of Plasmas* **14** (2007) 102903.

[22] P. F. Wyper and R. Jain. *Physics of Plasmas* **17** (2010) 092902.

[23] C. E. Parnell, R. C. Maclean and A. L. Haynes. *The Astrophysical Journal* **725** (2010b) L214.

[24] J. E. H. Stevenson, C. E. Parnell, E. R. Priest and A. L. Haynes. *Astronomy and Astrophysics* **573** (2015) A44.

[25] N. A. Murphy and C. R. Sovinec. *Physics of Plasmas* **15** (2008) 042313.

[26] N. A. Murphy, M. P. Miralles, C. L. Pope, J. C. Raymond, H. D. Winter, K. K. Reeves, D. B. Seaton, A. A. van Ballegooijen and J. Lin. *The Astrophysical Journal* **751** (2012) 56.

[27] G. Paschmann, M. Øieroset and T. Phan. *Space Science Reviews* **178** (2013) 385.

[28] M. Yamada, H. Ji, S. Hsu, T. Carter, R. Kulsrud, N. Bretz, F. Jobes, Y. Ono and F. Perkins. *Physics of Plasmas* **4**, (1997) 1936.

[29] P. F. Wyper and R. Jain. *Physics of Plasmas* **20** (2013) 052901.

[30] P. F. Wyper, R. Jain and D. I. Pontin. *Astronomy and Astrophysics* **545** (2012) A78.

[31] A. K. Al-Hachami and D. I. Pontin. *Astronomy and Astrophysics* **512** (2010) A84.

[32] K. Galsgaard and D. I. Pontin. *Astronomy and Astrophysics* **534** (2011) A2.

[33] J. A. Miller, P. J. Cargill, A. G. Emslie, G. D. Holman, B. R. Dennis, T. N. LaRosa, R. M. Winglee, S. G. Benka and S. Tsuneta. *Journal of Geophysical Research: Space Physics* **102** (1997) 14631.

[34] V. Petrosian and A. M. Bykov. *Space Science Reviews* **134** (2008) 207.

[35] A. M. Raadu. *Physics and Chemistry of the Earth, Part C: Solar, Terrestrial and Planetary Science* **26** (2001) 55.

[36] R. P. Lin and H. S. Hudson. *Solar Physics* **50** (1976) 153.

[37] R. P. Lin, S. Krucker, G. J. Hurford, D. M. Smith, H. S. Hudson, G. D. Holman, R. A. Schwartz, B. R. Dennis, G. H. Share, R. J. Murphy, A. G. Emslie, C. Johns-Krull and N. Vilmer. *The Astrophysical Journal* **595** (2003) L69.

[38] J. P. Eastwood, M. A. Shay, T. D. Phan and M. Øieroset. *Physical Review Letters* **104** (2010) 205001.

[39] Yu. V. Khotyaintsev, D. B. Graham, C. Norgren, E. Eriksson, W. Li, A. Johlander, A. Vaivads, M. André, P. L. Pritchett, A. Retinò, T. D. Phan, R. E. Ergun, K. Goodrich, P.-A. Lindqvist, G. T. Marklund, O. Le Contel, F. Plaschke, W. Magnes, R. J. Strangeway, C. T. Russell, H. Vaith, M. R.

Argall, C. A. Kletzing, R. Nakamura, R. B. Torbert, W. R. Paterson, D. J. Gershman, J. C. Dorelli, L. A. Avanov, B. Lavraud, Y. Saito, B. L. Giles, C. J. Pollock, D. L. Turner, J. D. Blake, J. F. Fennell, A. Jaynes, B. H. Mauk and J. L. Burch. *Geophysical Research Letters* **43** (2016) 5571.

[40] S. Dalla and P.K. Browning. *Astronomy and Astrophysics* **436** (2005) 1103.

[41] S. Dalla and P.K. Browning. *The Astrophysical Journal* **640** (2006) L99.

[42] S. Dalla and P. K. Browning. *Astronomy and Astrophysics* **491** (2008) 289.

[43] V.V. Zharkova and M. Gordovskyy. *The Astrophysical Journal* **604** (2004) 884.

[44] V.V. Zharkova and M. Gordovskyy. *Monthly Notices of the Royal Astronomical Society* **356** (2005) 1107.

[45] M. Hosseinpour. *Monthly Notices of the Royal Astronomical Society* **445** (2014a) 2476.

[46] M. Hosseinpour. *Astrophysics and Space Science* **353** (2014b) 379.

[47] M. Hosseinpour, M. Mehdizade and M. A. Mohammadi. *Physics of Plasmas* **21** (2014) 102904.

[48] Z. Akbari, M. Hossienpour and M. A. Mohammadi. *Journal of Plasma Physics* **82** (2016b) 905820509.

[49] Z. Akbari, M. Hossienpour and M. A. Mohammadi. *Astrophysics and Space Science* **361** (2016a) 355.

[50] P. Foukal, P. Miller and L. Gilliam. *Solar Physics* **83** (1983) 83.

[51] W. Davis. *Solar Physics* **54** (1977) 139.

[52] P. Foukal, R. Little and L. Gilliam. *Solar Physics* **114** (1988) 65.

[53] M. I. Pudovkin, S. A. Zaitseva, N. O. Shumilov and C.-V. Meister. *Solar Physics* **178** (1998) 125.

[54] M. Hosseinpour. *Astrophysics and Space Science* **358** (2015) 40.

Table 1: Injection positions of a proton from the second and forth quadrants.

Case	x	y	r	z
1	-0.1	-0.02	0.1	0.99
2	0.5	0.53	0.72	-0.56
3	0.22	0.80	0.83	-0.46
4	-0.28	-0.15	0.31	0.29
5	-0.46	-0.85	0.96	-0.52
6	-0.56	-0.52	0.76	-0.67
7	0.97	0.57	1.12	0.38

Table 2: Injection positions of a proton from the first and third quadrants.

Case	x	y	r	z
8	0.33	-0.86	0.92	-0.66
9	-0.51	0.71	0.87	-0.98
10	-0.52	0.74	0.90	0.74
11	0.58	-0.90	1	0.18
12	0.62	-0.97	1.15	-0.35
13	0.77	-0.83	1.13	0.83
14	-0.92	0.90	1.28	-0.89

Table 3: Injection positions of a proton with constant z.

Case	x	y	r	z
1	0.01	0.03	0.2	0.3
2	0.25	0.75	0.5	0.3
3	0.35	1.05	0.7	0.3
4	0.45	1.35	0.9	0.3

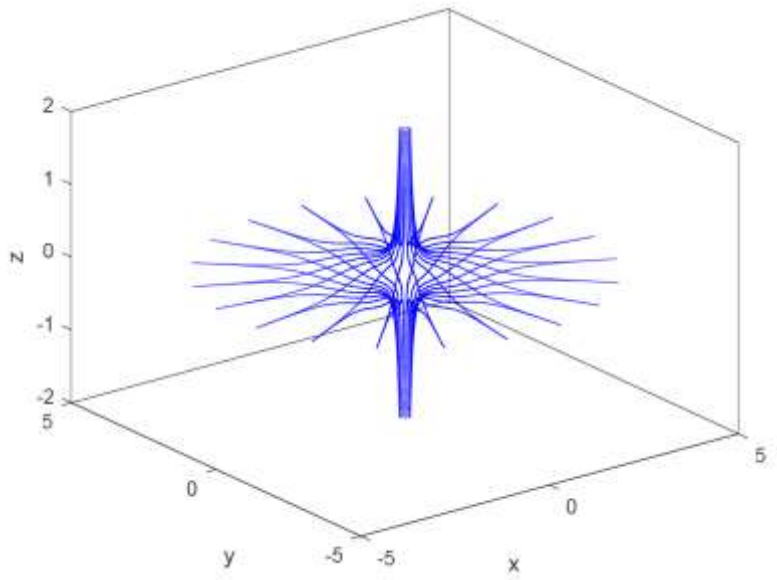

Figure1: Plot of magnetic field lines for spine reconnection with $b_0 = L_0 = j = 1$ and $m = 0.5$.

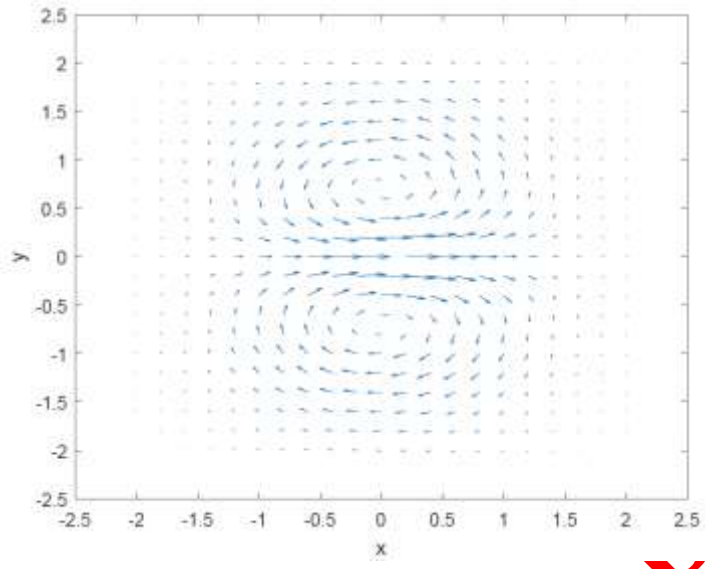

(a)

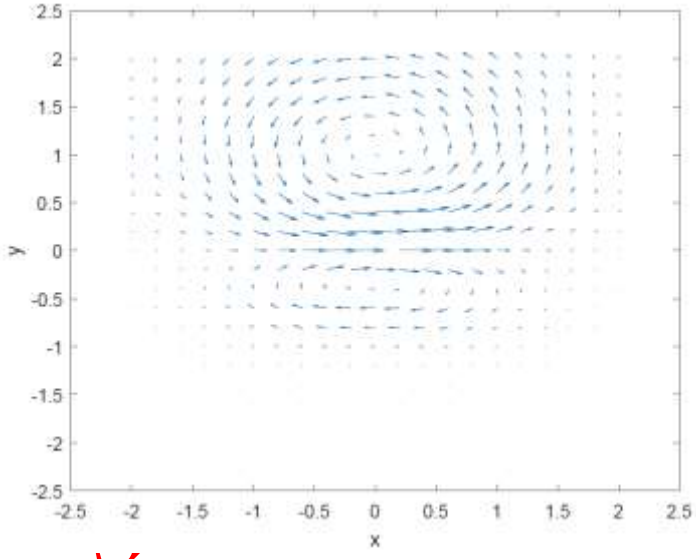

(b)

Figure 2: The vector plot of electric current density with $b_0 = L_0 = \mu_0 = j = 1$ and (a) $m = 0$ (b) $m = 0.5$.

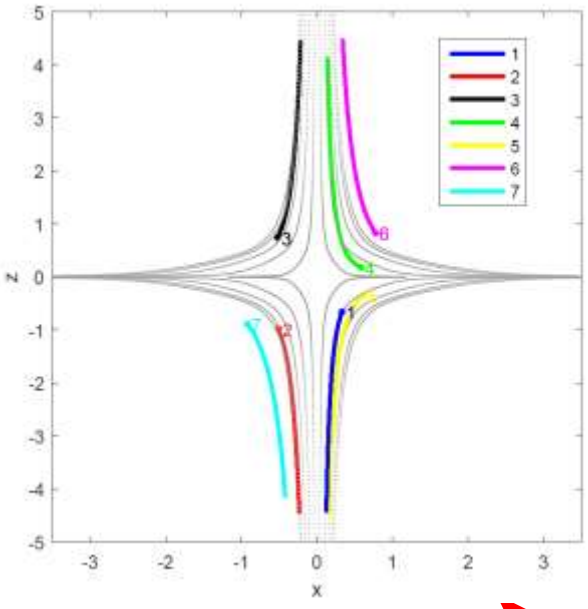

Figure 3: The trajectory of a proton with initial positions listed in table 1 with $E_0 = 1\ kV/m$ and $B_0 = 0.01\ T$.

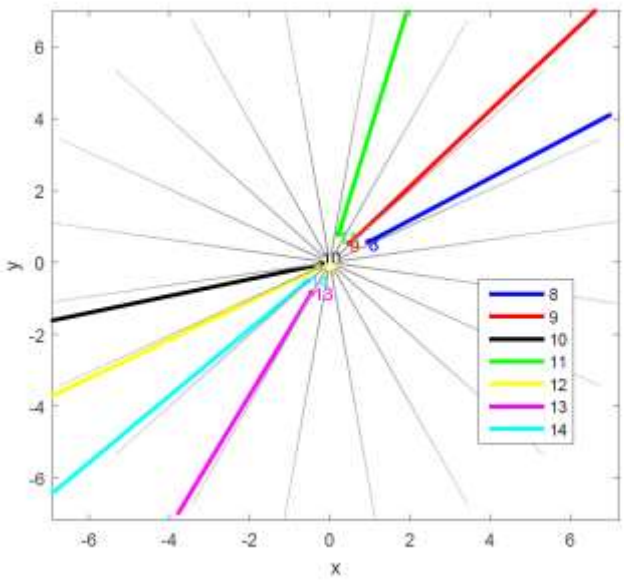

Figure 4: The trajectory of a proton with initial positions listed in table 2 with $E_0 = 1\ kV/m$ and $B_0 = 0.01\ T$.

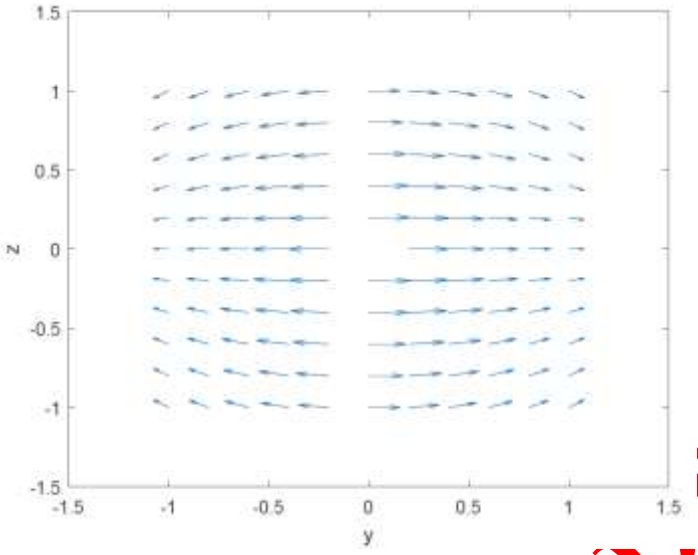

(a)

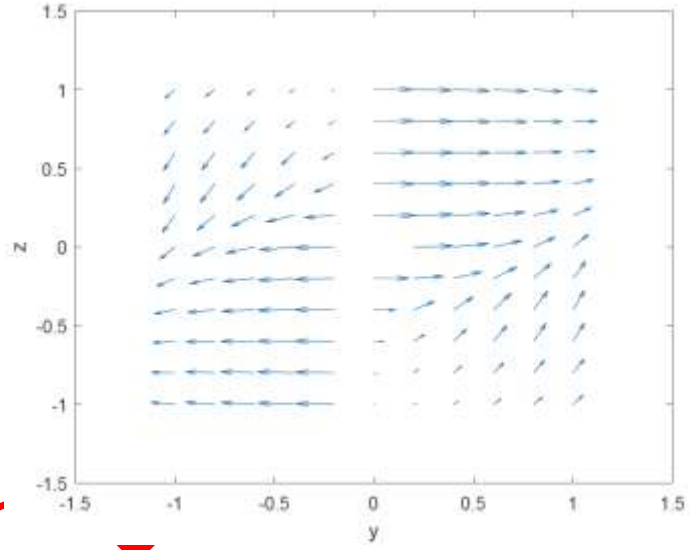

(b)

Figure 5: Vector plots of the electric field (Eq. 8) at $z = 0$ plane, (a) $m = 0$ (b) $m = 0.5$.

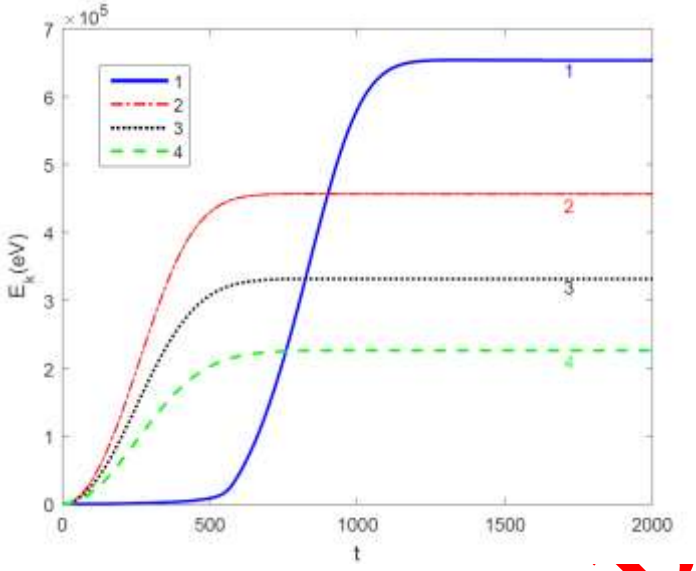

Figure 6: Time variation of kinetic energy of a proton with initial points listed in table 3 $E_0 = 1\ kV/m$ and $B_0' = 0.01\ T$.

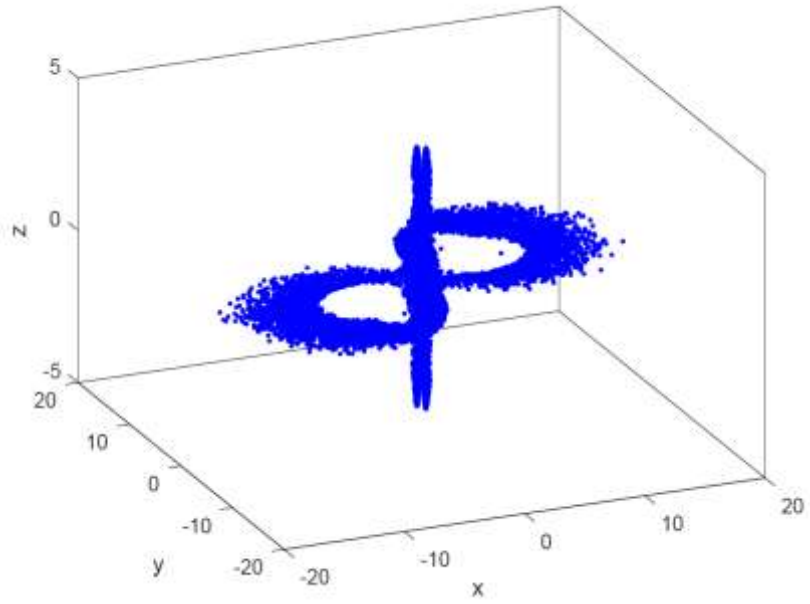

Figure 7: Final distribution of particles.

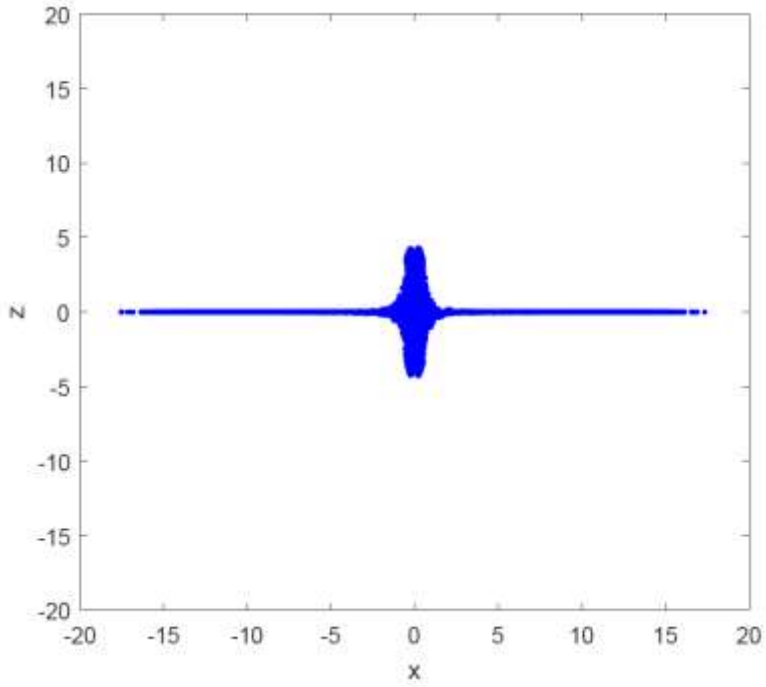

Figure 8: Final position of particles in the $(x - z)$ plane.

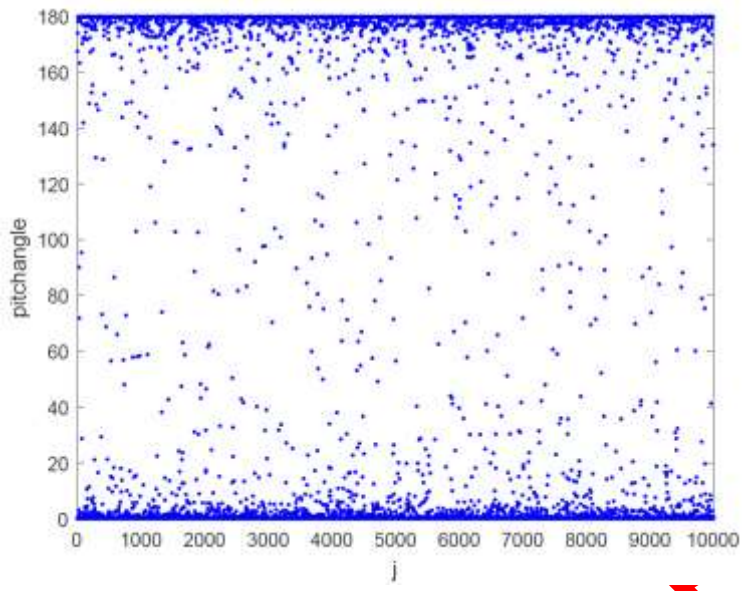

Figure 9: Final pitch angle of particles with $m = 0.5$.

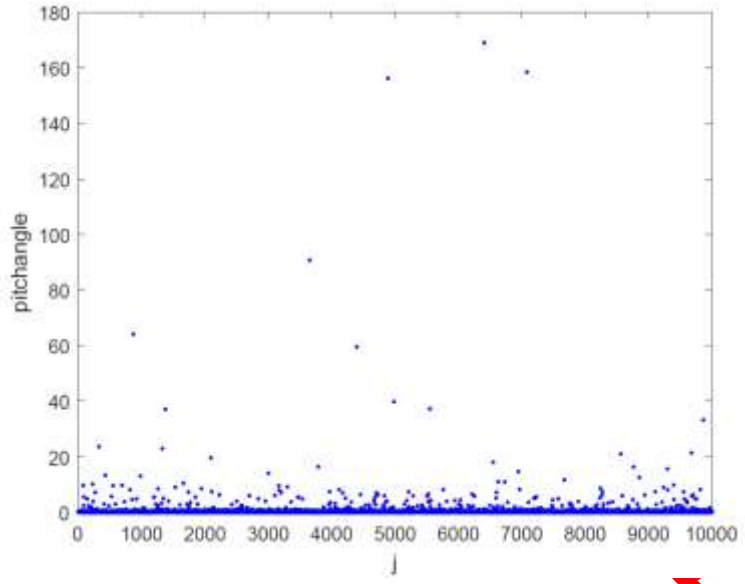

(a)

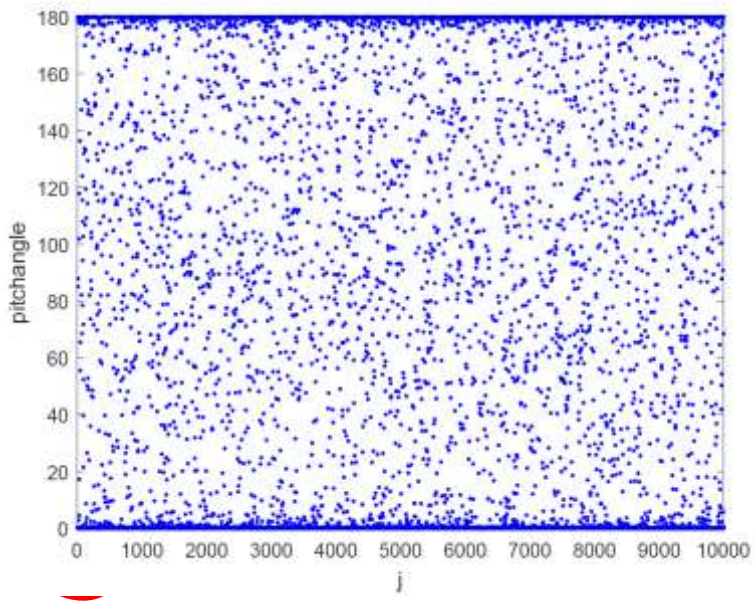

(b)

Figure 10: Final pitch angle of particles, (a) $m = 0$ (b) $m = 1$.

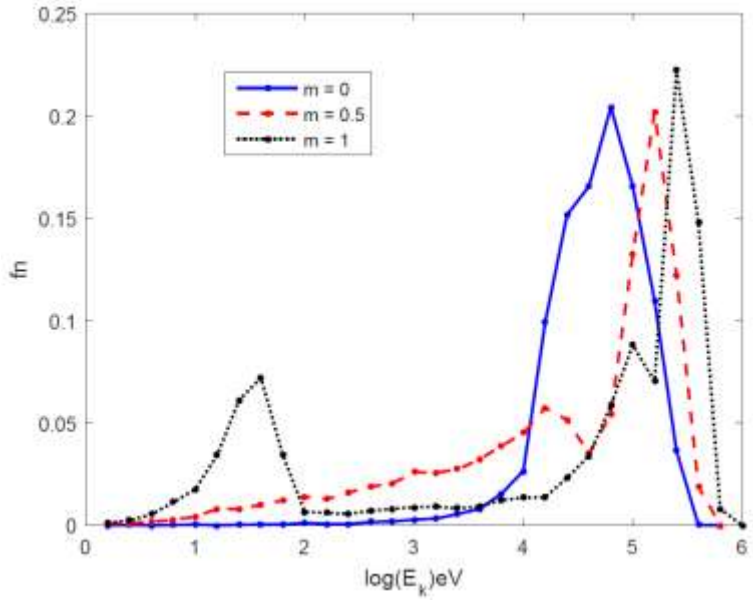

Figure 11: Energy distribution of particles for $m = 0, 0.5, 1$ with $B_0' = 0.01\ T$ and $E_0 = 1\ kV/m$.

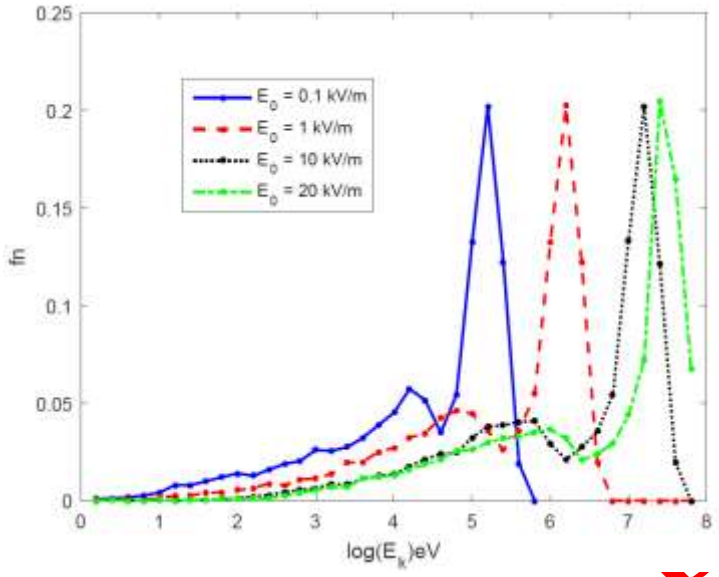

Figure 12: Energy distribution of particles for different values of E_0 with $B_0' = 0.01\ T$.

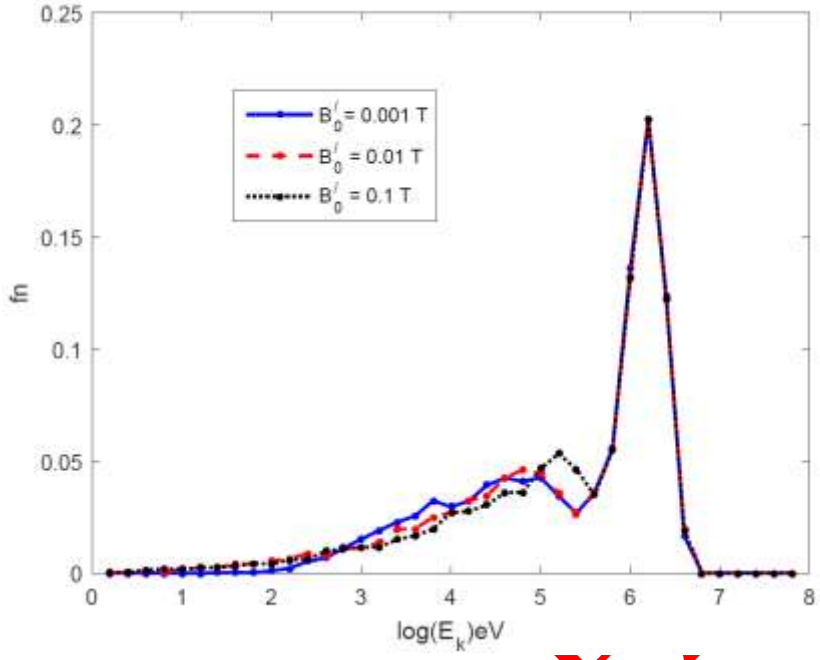

Figure 13: Energy distribution of particles for different values of B_0' with $E_0 = 1\ kV/m$.